Preparation and Properties of Core–Shell Nanosilica/Poly(methyl methacrylate–butyl acrylate–2,2,2-trifluoroethyl methacrylate) Latex

Zheng Wei, He Ling, Liang Junyan, Chang Gang, Wang Na

School of Science, Xi'an Jiaotong University, Xi'an 710049, China

Received 14 May 2009; accepted 24 June 2010
DOI 10.1002/app.33000
Published online 9 November 2010 in Wiley Online Library (wileyonlinelibrary.com).

ABSTRACT: A core–shell nanosilica (nano-SiO_2)/fluorinated acrylic copolymer latex, where nano-SiO_2 served as the core and a copolymer of butyl acrylate, methyl methacrylate, and 2,2,2-trifluoroethyl methacrylate (TFEMA) served as the shell, was synthesized in this study by seed emulsion polymerization. The compatibility between the core and shell was enhanced by the introduction of vinyl trimethoxysilane on the surface of nano-SiO_2. The morphology and particle size of the nano-SiO_2/poly(methyl methacrylate–butyl acrylate–2,2,2-trifluoroethyl methacrylate) [P(MMA–BA–TFEMA)] core–shell latex were characterized by transmission electron microscopy. The properties and surface energy of films formed by the nano-SiO_2/P(MMA–BA–TFEMA) latex were analyzed by Fourier transform infrared spectroscopy, differential scanning calorimetry, thermogravimetric analysis, scanning electron microscopy/energy-dispersive X-ray spectroscopy, and static contact angle measurement. The analyzed results indicate that the nano-SiO_2/P(MMA–BA–TFEMA) latex presented uniform spherical core–shell particles about 45 nm in diameter. Favorable characteristics in the latex film and the lowest surface energy were obtained with 30 wt % TFEMA; this was due to the optimal migration of fluorine to the surface during film formation. The mechanical properties of the films were significantly improved by 1.0–1.5 wt % modified nano-SiO_2. © 2010 Wiley Periodicals, Inc. J Appl Polym Sci 120: 1152–1161, 2011

Key words: composites; core–shell polymers; emulsion polymerization; films

INTRODUCTION

Inorganic/organic hybrid materials possess the advantages of both the inorganic material and the organic polymer.[1,2] The incorporation of an inorganic phase into an organic polymer matrix may be an effective approach for enhancing the mechanical strength and may provide improvements over other specific properties of the organic polymer.[3–6]

Nanosilica (nano-SiO_2)/fluorinated acrylic copolymers are typical inorganic/organic hybrid materials. The synergism of advantageous properties between nano-SiO_2 and fluorinated acrylic copolymers provides it with excellent properties, such as a low surface energy, thermal stability, hydrophobic behaviors endowed by fluorinated acrylic copolymers, and a high strength endowed by nano-SiO_2.[7–9] Therefore, up to this point, nano-SiO_2/fluorinated acrylic copolymers have attracted much attention in the field of protective coatings.[10,11]

In fact, the final properties of these nano-SiO_2/fluorinated acrylic copolymers materials are strongly dependent on the structural design, such as blends and core–shell structures, of the components. When nano-SiO_2/fluorinated acrylic copolymers are designed with a core–shell structure, especially when nano-SiO_2 serves as the core and fluorinated acrylic copolymers serve as the shell (this is referred to as a core–shell nano-SiO_2/fluorinated acrylic copolymer latex), the differences in compatibility between silicon and fluorine and the polar interactions between the core versus the substrate and the shell versus the substrate could drive the fluorinated groups to preferentially migrate to the film surface and nano-SiO_2 to disperse into the polymer matrix. From this point of view, such migration and rearrangement of the components not only maintains the excellent surface properties of the film materials, even in a low amount of fluorine, but also improves the mechanical properties of the films by nano-SiO_2.[12,13]

However, making a core–shell nano-SiO_2/fluorinated acrylic copolymer latex is not trivial. Thermodynamic instability is created by the different hydrophobic properties and weak bonding forces between the more polar core and the less polar shell; this induces the transformation between the core and shell, even obvious macrophase separation, and ultimately affects the superior performance of the latex

Correspondence to: H. Ling (heling@mail.xjtu.edu.cn).
Contract grant sponsor: National Science Foundation of China; contract grant number: 20474050.

film. On the other hand, a multinuclear structure rather than single core structure is normally obtained because of the small size and high surface energy of nano-SiO_2.[10] It is, therefore, promising to modify the nano-SiO_2 surface with modifier agents (i.e., silane coupling agent) to enhance the interaction between the nano-SiO_2 core and the fluorinated acrylic copolymers shell[14,15] and to employ the semicontinuous emulsion polymerization technique to synthesize core–shell particles with a single core.[12] Silica sol usually serves as the core of nano-SiO_2/fluorinated acrylic copolymer latex to improve the properties of the latex. However, fumed nano-SiO_2, compared with nano-SiO_2 obtained by silica precursors (tetraethylorthosilicate) via the sol–gel process,[16,17] has an extremely large surface area and a smooth nonporous surface and can cause different effects or mechanisms from that of silica sol. Additionally, the direct use of fume nano-SiO_2 simplifies the procedure for the *in situ* synthesis of SiO_2 and provides more suitable surface properties of the final material.[18] Nevertheless, to this point, there has been a lack of study of core–shell nano-SiO_2/fluorinated acrylic copolymers with fumed nano-SiO_2 as the core because this development was extremely limited by the difficulty obtaining a stable dispersion for the encapsulation of fumed nano-SiO_2 because silanol and siloxane bonds usually hold individual fumed silica particles in aggregation even under the best mixing conditions.[19]

The aim of this study was to obtain a core–shell structure latex by a morphogenetic control method. Fumed nano-SiO_2 was used as the core after ultrasonic dispersion and surface modification, and the polymer shell gradually took shape via semicontinuous seed emulsion polymerization. The final morphology of the core–shell nano-SiO_2/poly(methyl methacrylate–butyl acrylate–2,2,2-trifluoroethyl methacrylate) [P(MMA–BA–TFEMA)] latex and the film properties were characterized by transmission electron microscopy (TEM), Fourier transform infrared (FTIR) spectroscopy, scanning electron microscopy/energy-dispersive X-ray spectroscopy (SEM–EDX), differential scanning calorimetry (DSC), thermogravimetric analysis (TGA), static contact angle measurement, and mechanical testing.

EXPERIMENTAL

Materials

2,2,2-Trifluoroethyl methacrylate (TFEMA) and vinyl trimethoxysilane (VTMS) were supplied by XEOGIA Fluorine-Silicon Chemical Co. Ltd. (Harbin, China) and Wuhan University Silicone New material Co. Ltd. (Wuhan, China), respectively. Nano-SiO_2 (VK-SP15), with an average diameter of 10–25 nm (determined by TEM) and a specific area of 230 m^2/g, was supplied by Hang Zhou Wan Jing New Material Co. Ltd. (Hang Zhou, China). Methyl methacrylate (MMA) and *n*-butyl acrylate (BA), supplied by Aldrich were rinsed with a 10 wt % NaOH aqueous solution and ion-free water until the pH value of the rinse water was about 7; They were then dried over anhydrous magnesium sulfate for 24 h. Concentrated hydrochloride (36%vol), isopropyl alcohol, sodium dodecyl sulfate (SDS), octylphenyl polyoxyethylene ether (TX-10), sodium bicarbonate, and ammonium persulfate (APS) in analytical purity were purchased commercially and were used as received.

Preparation of the nano-SiO_2/P(MMA–BA–TFEMA) core–shell latex

Surface modification of nano-SiO_2

In 220 mL of a water/isopropyl alcohol solution (5/6 v/v), 4.0 g of nano-SiO_2 was well suspended by sonication of the resulting mixture for 40 min. Then, 4.0 g of VTMS was added to the obtained suspension, and the pH was adjusted to 3–4 with a concentrated HCl solution. The mixture was immediately transferred into a four-mouthed flask equipped with a reflux condenser and a mechanical stirrer; this was followed by vigorous stirring for 1 h at 82°C under a nitrogen atmosphere. The solid modified SiO_2 was obtained after the suspension was cooled to room temperature and the liquid phase was removed by centrifugation. Then, the modified SiO_2 particles were extracted with acetone for 4 h in a Soxhlet extractor to remove unreacted chemicals; this was followed by drying at 100°C for 1 h under reduced pressure. The dried modified SiO_2 particles were ground into fine powder before use.

Synthesis of the nano-SiO_2/P(MMA–BA–TFEMA) core–shell latex

The nano-SiO_2/P(MMA–BA–TFEMA) core–shell latex was prepared by the following procedure: The modified nano-SiO_2 fine powder, together with mixed emulsifiers (TX-10/SDS weight ratio = 2:1), was ultrasonically dispersed into ion-free water to prepare the seed latex. The seed latex was added to a flask under a nitrogen atmosphere and heated to 75°C; this was followed by the introduction of $NaHCO_3$ and APS solutions into the flask successively under vigorously stirring. Then, a mixture of monomer MMA, BA, and TFEMA was slowly added to the flask dropwise over 4 h. The reaction temperature was held at 80°C for 2 h more before the nano-SiO_2/P(MMA–BA–TFEMA) core–shell latex was obtained. The recipes for the nano-SiO_2/P(MMA–BA–TFEMA) core–shell latex are given in Table I.

TABLE I
Recipes for the Synthesis of the Core–Shell Latex

Sample[a]	Modified SiO_2 (g)	BA (g)	MMA (g)	TFEMA (g)	TX-10 (g)	SDS (g)	APS (g)	$NaHCO_3$ (g)	Water (g)
N1	0.1	10.3	7.8	2.0	1.6	0.8	0.10	0.03	60
N2	0.1	9.1	6.9	4.0	1.6	0.8	0.10	0.03	60
N3	0.1	8.6	6.4	5.0	1.6	0.8	0.10	0.03	60
N4	0.1	8.0	6.0	6.0	1.6	0.8	0.10	0.03	60
N5	0.1	6.9	5.1	8.0	1.6	0.8	0.10	0.03	60
N6	0.1	5.7	4.2	10.0	1.6	0.8	0.10	0.03	60
S1	0.1	6.0	8.0	6.0	1.8	0.9	0.10	0.03	60
S2	0.2	6.0	8.0	6.0	1.8	0.9	0.10	0.03	60
S3	0.3	6.0	8.0	6.0	1.8	0.9	0.10	0.03	60
S4	0.4	6.0	8.0	6.0	1.8	0.9	0.10	0.03	60
S5	0.5	6.0	8.0	6.0	1.8	0.9	0.10	0.03	60

[a] In the sample codes, "N" indicates different contents of TFEMA, and "S" indicates different contents of modified SiO2.

Characterization of the core–shell latex and the copolymer film

FTIR spectra of the modified SiO_2, nano-SiO_2, and core–shell latex films were recorded on an Avatar 360 FTIR spectrometer (Nicolet Co., Wisconsin) in the range 4000–400 cm^{-1}. A JEM-3010 transmission electron microscope (JEOL Ltd., Tokyo, Japan) with an acceleration voltage of 200 kV was used for the morphology study of the latex nanoparticles. The obtained latexes were diluted with ion-free water and then deposited onto carbon-coated copper grids after they were dyed with a phosphotungstic acid solution. TEM observations were performed after the grids were dried in air. The morphology of the film surface, the film cross section, and its elemental composition were obtained with a JSM-6460 scanning electron microscope (JEOL Ltd., Tokyo, Japan) coupled with an energy-dispersive X-ray detector for electron-beam microprobe analysis. The determination of the elemental composition was carried out at an acceleration voltage of 25–30 keV, a lifetime greater than 50 s, a pulse-counting rate of about 2000 cps, and a working distance of 34 mm. DSC analysis was carried out on a DSC-200 instrument (Netzsch, Co. Ltd., Bavaria, Germany). The samples were preheated to 100°C for 5 min to eliminate the thermal history, quickly cooled to −80°C, and finally heated to 300°C at a heating rate of 10°C/min under a nitrogen atmosphere. The thermogravimetric data were obtained from a Q600 thermogravimetry analyzer (TA Instruments Inc., New Castle, USA) under a dry nitrogen atmosphere over the temperature range 25–700°C at a heating rate of 10°C/min. The measurements were taken with 10–11 mg of film samples. The static contact angles of the films were measured with a JC2000C2 contact angle goniometer (Zhongchen Power Co., Shanghai, China) by the sessile drop method with a microsyringe at 25°C. The injection volume of liquid was 5 μL, and the average of six readings of contact angles were used as the final value for each sample. The surface free energies of different samples were evaluated via the following equations:

$$\gamma_l(1+\cos\theta) = 2\left[\left(\gamma_l^d\gamma_s^d\right)^{1/2} + \left(\gamma_l^p\gamma_s^p\right)^{1/2}\right] \quad (1)$$

$$\gamma_s = \gamma_s^d + \gamma_s^p \quad (2)$$

where θ is the static contact angle of the liquid on the film surface; γ_l and γ_s are the surface tensions of the liquid and solid, respectively; γ_l^p and γ_l^d are the polar and dispersive components of the liquid surface tension, respectively; and γ_s^p, and γ_s^d are the polar and dispersive components of the solid surface tension, respectively. γ_s^d and γ_s^p were calculated with the contact angles, surface tension, and dispersion and polar components of water (γ_l = 72.8 mN/m, γ_l^p = 21.8 mN/m, and γ_l^p = 51.0 mN/m) and hexadecane (γ_l = 27.6 mN/m, γ_l^d = 27.6 mN/m, and γ_l^p = 0 mN/m). The tensile strength and fracture elongation of the films were measured with a tensile testing machine CMT6503 (SANS Co., Cheng De, China).

RESULTS AND DISCUSSION

Characterization of the core–shell latex

The obtained construction structures of the nano-SiO_2/P(MMA–BA–TFEMA) latex particles were characterized with TEM images, as shown in Figure 1. Typical core–shell structures were observed via the significant contrast between the core (light regions) and shell (dark regions) because of their differences in electron penetrability [Fig. 1(a)]. The thickness of the P(MMA–BA–TFEMA) shell in the core–shell particles was about 5 nm, which was rather small compared with the average diameter of the whole particles. As shown in Figure 1(b), the

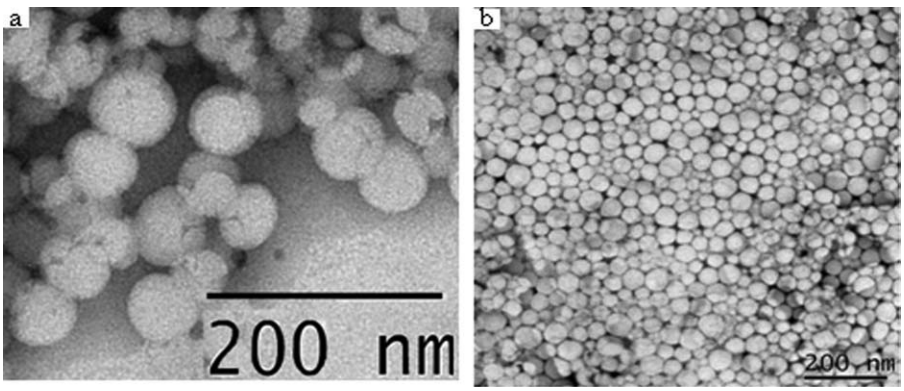

Figure 1 TEM images of nano-SiO_2/P(MMA–BA–TFEMA) latex particles (N4) with 30 wt % TFEMA (image a is an enlargement of part of image b).

distribution of particle size was relatively homogeneous, and the average diameter of the core–shell particles was about 45 nm.

The additional amount of modified SiO_2 had a great influence on the structure of the latex particles. As shown in Figure 2, the construction structures of

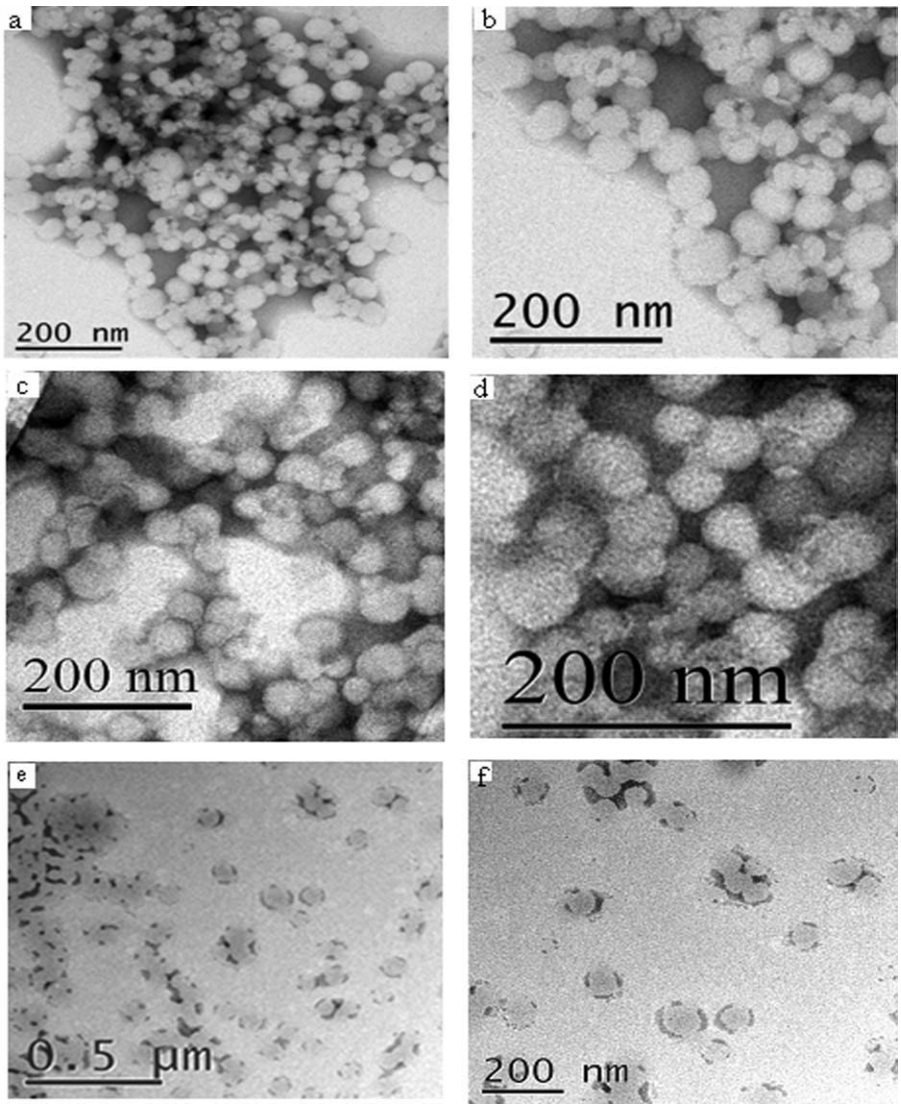

Figure 2 TEM images of latex particles with different contents of modified SiO_2 (S1, S4, and S5): (a,b) 0.5, (c,d) 2.0, and (e,f) 2.5 wt %.

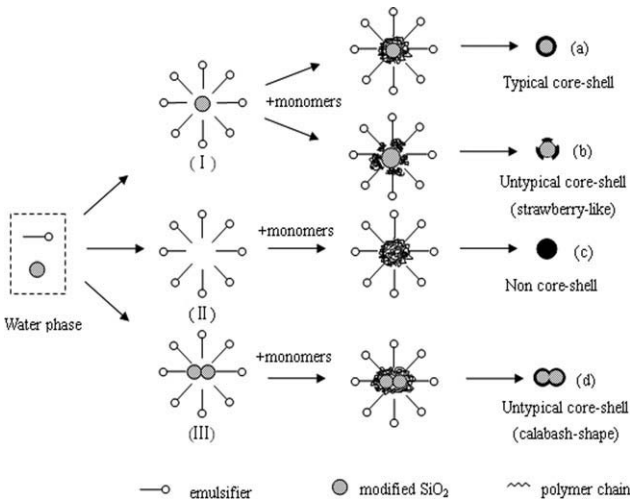

Figure 3 Schematic diagram of the formation of nano-SiO_2/P(MMA–BA–TFEMA) latexes with different structures.

the three latex particle samples prepared with varied modified SiO_2 contents were compared. When the amount of modified SiO_2 was 0.5 wt %, the core–shell composite particles with a continuous shell in majority, together with a few neat copolymer particles, expressed as all-black spheres, were formed [Fig. 2(a,b)]. Meanwhile, most of the modified SiO_2 particles were covered by P(MMA–BA–TFEMA). When the amount of modified SiO_2 was increased to 2.0 wt %, the polymer shell of the latex particles became discontinuous, and obvious conglutination occurred among composite particles, as shown in Figure 2(c,d). Some modified SiO_2 beads were even observed to link together and form a calabash shape. Further increases in the additional content of modified SiO_2 to 2.5 wt % resulted in an even thinner polymer shell and serious conglutination among the composite particles. Some strawberry-like composite particles and aggregates, because of serious conglutination between particles, were observed, as shown in Figure 2(e,f), but no neat polymer particles were observed in this sample.

From this analysis, the deduced nano-SiO_2/P(MMA–BA–TFEMA) latexes with different structures are illustrated schematically following the emulsion polymerization mechanism in Figure 3. The modified nano-SiO_2 and surfactant dispersed in the water phase coexisted in three forms: (I) a micelle containing a single nano-SiO_2, (II) a hollow micelle without nano-SiO_2, and (III) a micelle containing several nano-SiO_2's. The micelles containing a single nano-SiO_2 (form I) as seeds were first formed once the modified nano-SiO_2 and surfactant were dispersed in the water phase. The following added monomers in the hydrophobic phase entered the micelles and were polymerized in the presence of an initiator at certain temperature. Therefore, the core–shell structure composite particles [Fig. 3(a)] were formed. When the amount of nano-SiO_2 was relatively low (e.g., 0.5 wt %), the surfactant was more than enough to disperse all of the nano-SiO_2 particles evenly. As a result, some hollow micelles containing no nano-SiO_2 (form II) might have been formed. The monomers filled these hollow micelles and were polymerized in the presence of initiator as well. Therefore, neat polymer particles [Fig. 3(c)] were formed, as previously shown in Figure 2(a,b). Meanwhile, the well-dispersed seed micelles containing nano-SiO_2 formed uniform core–shell particles after the polymerization of the monomer. With increasing nano-SiO_2 content, the hollow micelles formed in the first stage decreased continuously. When the surfactant was not sufficient, some micelles containing more than one nano-SiO_2 particle (form III) might have been formed. As a result, the conglutination among composite particles happened after the polymerization of the monomer, and calabash-shaped particles [Fig. 3(d)] were formed; this agreed with the observations shown in Figure 2(c,d). The additional increase of the nano-SiO_2 content to 2.5 wt % resulted in the formation of strawberry-like particles [Fig. 3(b)] because of the monomers were insufficient to form a noncontinuous shell polymer, and even more serious conglutination between the particles occurred. Meanwhile, no hollow micelles were formed in the first stage; therefore, no neat polymer was produced in the final sample accordingly. In this case, the optimized nano-SiO_2 content existed to form perfect core–shell particles without either conglutination or neat polymer particles in the fixed surfactant and monomer feedings.

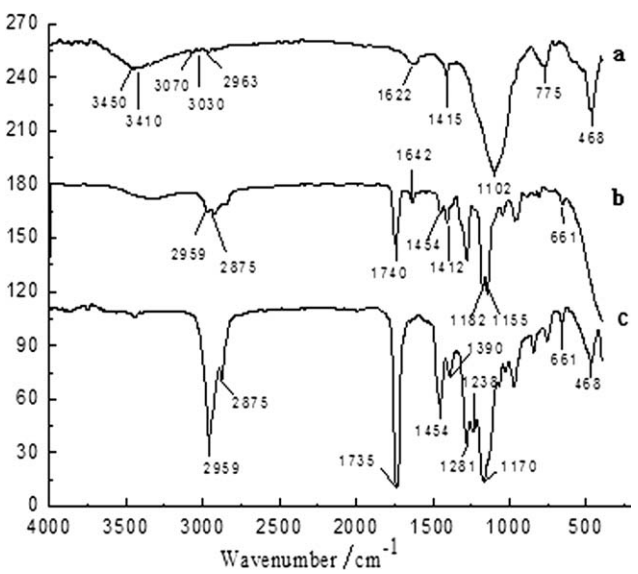

Figure 4 FTIR spectra of (a) modified nano-SiO_2, (b) TFEMA, and (c) core–shell nano-SiO_2/P(MMA–BA–TFEMA) latex N4.

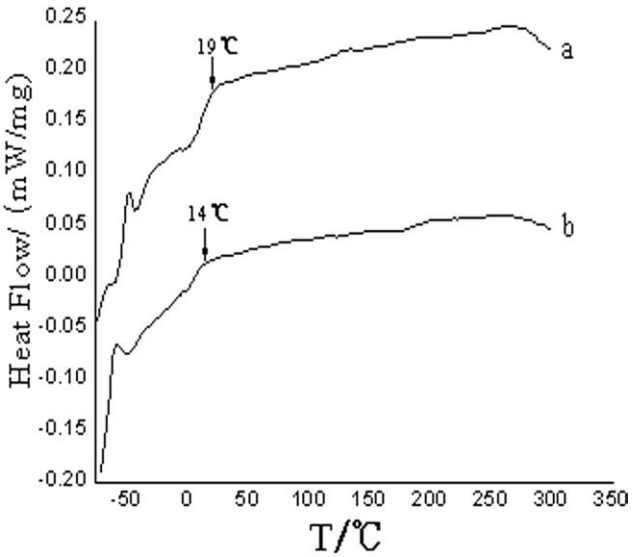

Figure 5 DSC curves for (a) the blend latex and (b) core–shell latex S3 (T = temperature).

Figure 4 shows the FTIR spectra of the modified nano-SiO_2, TFEMA, and core–shell nano-SiO_2/fluorinated acrylic copolymer latex film N4. For modified nano-SiO_2 [Fig. 4(a)], the board peak at 3410–3450 cm^{-1} was due to the O—H group (Si—OH). The peaks at 3070 and 3030 cm^{-1} were attributed to the stretching vibration of the vinyl group (C=C), and the peak at 2963 cm^{-1} was the characteristic peak of the C—H (CH_3) group. The peaks at 1622 and 1415 cm^{-1} were assigned to the stretching vibration and bending vibration, respectively, of the vinyl group, and the peaks at 1102 and 468 cm^{-1} corresponded to the asymmetric stretching vibration and the bending vibration, respectively, of the Si—O—Si bond. The existence of vinyl groups confirmed that the VTMS coupling agents were chemically coated onto the surface of the nano-SiO_2 particles. Figure 4(b) presents the FTIR spectra of TFEMA. The peaks at 2959 and 2875 cm^{-1} were the characteristic stretching peaks of the C—H (CH_2) group. The peak at 1740 cm^{-1} was the stretching vibration of the C=O group, and the peaks at 1642 and 1412 cm^{-1} corresponded to the stretching vibration and bending vibration, respectively, of the vinyl group. The characteristic peaks of CF_3 were at 1282 cm^{-1}. The distortion vibration of CH_2 was at 1454 cm^{-1}. The asymmetric and symmetric stretching vibrations of the (O=)C—O—C group were at 1182–1155 and 1055 cm^{-1}, respectively. The peak at 661 cm^{-1} was the wagging vibration of C—F (CF_3) group. Figure 4(c) shows the FTIR spectra of the core–shell nano-SiO_2/fluorinated acrylic copolymer latex film. Compared with Figure 4(a,b), the major differences in the characteristic peaks for the nano-SiO_2/P(MMA–BA–TFEMA) were as follows. The characteristic stretching peaks of C—H at 2959 and 2875 cm^{-1} were much stronger, whereas the feature peaks of the vinyl group at about 1600 and 1415 cm^{-1} disappeared; this indicated the polymerization of the vinyl group on the surface of nano-SiO_2 with the monomers. The appearance of the stretching vibration and wagging vibration of the C—F (CF_3) group at 1238 and 661 cm^{-1}, respectively, and the bending vibration of Si—O—Si at 468 cm^{-1} revealed that TFEMA and modified nano-SiO_2 were introduced into the latex particles. Furthermore, a series of evidence, including the band at 1281–1170 cm^{-1} due to the overlap of the stretching vibration of the C—F(CF_3) group [at 1282 cm^{-1} in Fig. 4(b)], the stretching modes of the C—O—C group [at 1182–1155 cm^{-1} in Fig. 4(b)], and the feature peak of the Si—O—Si group [at 1102 cm^{-1} in Fig. 4(a)], confirmed the core–shell structure formed, as illustrated in Figure 3.

The influence of the core–shell structure on the thermal properties of the hybrid materials was studied with DSC and TGA, as shown in Figures 5 and 6, respectively. For comparison purposes, a blend latex prepared by the simple mixing of nano-SiO_2 (1.5 wt %) and P(MMA–BA–TFEMA) was prepared. As shown in Figure 5, the glass-transition temperature of the core–shell nano-SiO_2/fluorinated acrylic copolymer latex film (S3) was [14°C, Fig. 5(b)] was 5°C lower than that of the simple blended latex film [19°C, Fig. 5(a)] because of their different construction structures. For the core–shell latex, the interface interaction between the nano-SiO_2 core and the polymer shell was greatly reduced because the nano-SiO_2 and polymer were chemically bonded by the VTMS bridge. The nano-SiO_2 core possessed fewer constraints to the chain segments in the polymer

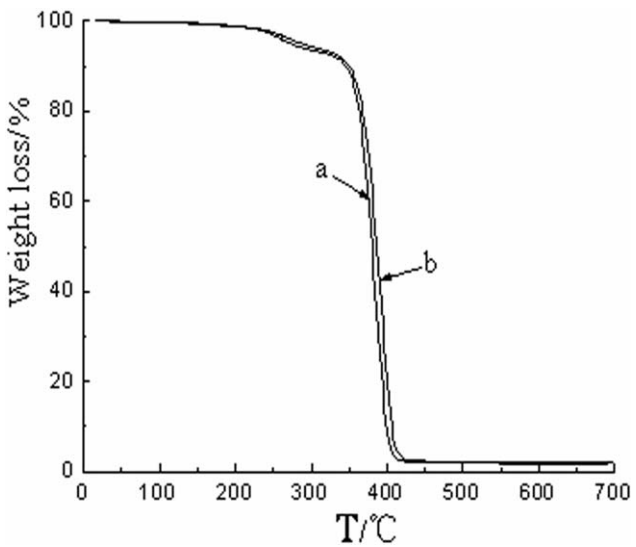

Figure 6 TGA curves for (a) the blend latex and (b) core–shell latex S3 (T = temperature).

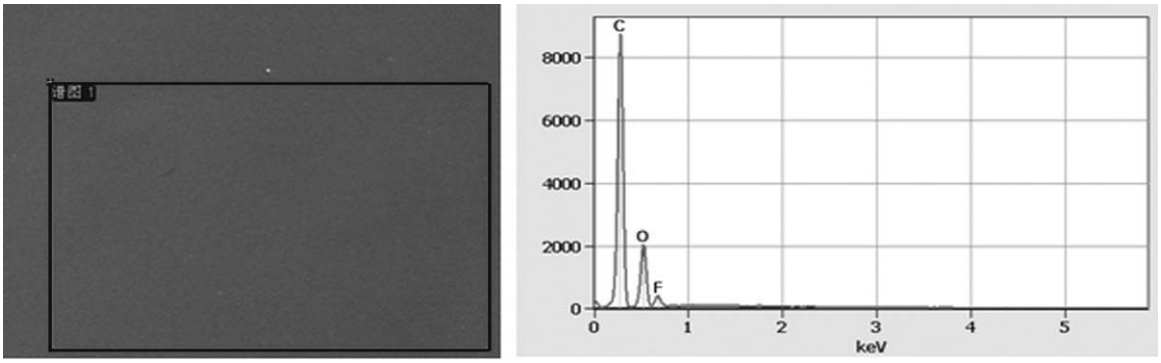

Figure 7 SEM–EDX images of the film formed from the latex.

shell. Therefore, a sufficient free volume might have been provided for the motion of the polymer segment, and a lower glass-transition temperature was observed in the core–shell latex film. As for the blending latex, nano-SiO_2 without surface modification would have been randomly dispersed in the polymer matrix, which might have greatly hindered the motion of the polymer segment for the high interface interaction between the nano-SiO_2 and polymer matrix. As a result, the free volume was reduced, whereas a higher glass-transition temperature was obtained. As a matter of fact, the core–shell structure was able to promote the polymer segmental motion; this might have been related to the fluorine preferential migration onto the film surface.

As shown in Figure 6, both the core–shell latex and the random blend latex had two degradation stages: one was at 300°C, corresponding to the chain-end decomposition of vinylidene,[20] and the other was approximately at 400°C and was due to the degradation of the main chain of the polyacrylate matrix. However, the decomposition temperature at the maximum weight loss rate of the core–shell latex reached 390°C, which was slightly higher than that of the blend latex (383°C). This might have been induced by the preferential migration of fluorine in the core–shell latex, which favored the formation of a film surface more tightly packed with —CF_3 than the random blend latex and provided its film with good resistance for the thermal degradation of the polymer matrix. Therefore, slightly higher thermal degradation temperatures of both stages were observed in the core–shell latex than in the random blend one.

Both DSC and TGA indicated that the preferential migration of fluorine onto the film surface was responsible for the better performance of the core–shell latex than blend one. The preferential migration of fluorine is discussed in detail later.

Surface characterization of the film

The fluorine migration onto the film surface was further confirmed with SEM–EDX, as shown in Figure 7. A cocontinuous film was obtained by the core–shell nano-SiO_2/fluorinated acrylic copolymer latex, and the major elements on the surface were carbon, oxygen, and fluorine. The fluorine content detected on the film surface was proportional to the TFEMA content and was higher than its theoretical value (Table II). It seemed that when more TFEMA was introduced, it might have resulted in a larger deviation of the fluorine content between the value detected on the surface and that calculated in theory. For example, the content of fluorine on the air-side surface of the film was 18.48 wt % by EDX, which was obviously higher than its theoretical value of 10.18 wt %. However, in samples N3 (25 wt % TFEMA) and N2 (20 wt % TFEMA), the amounts of fluorine on the air-side surface of the films were 10.55 and 7.39 wt %, respectively, just a little higher than their theoretical values of 8.04 and 6.79 wt %. This meant the fluorine migration indeed happened onto the film–air surface during the formation of the latex film. Because of the extremely low surface free energy and self-aggregation properties of the fluorine atoms in nature, the fluorinated side chains of a copolymer are capable of organizing into a well-ordered structure both in the bulk and at the surface in such a way that forms a surface primarily composed of tightly packed —CF_3 groups.[21] From a molecular-level perspective, a uniformly organized array of —CF_3 groups would be a surface with the lowest possible surface tension. In other respects, the

TABLE II
Elemental Compositions of the Film–Air Interfaces of Films with Different Contents of TFEMA and 0.5 wt % Modified SiO_2

TFEMA content with respect to the total monomers (wt %)	F (wt %)[a]	Si (wt %)
20 (N2)	7.39 (6.79)	–
25 (N3)	10.55 (8.04)	–
30 (N4)	18.48 (10.18)	–

[a] The theoretical values are presented within parentheses.

TABLE III
Elemental Compositions of Films with Different Contents of Modified SiO_2 and 25 wt % TFEMA

Modified SiO_2 content with respect to the total monomers (wt %)	F (wt %)			Si (wt %)[a]	
	Film–air interface	Average in bulk	Film–glass interface	Film–air interface	Film–glass interface
0.5 (S1)	10.55	8.37	11.40	–	0.17 (0.23)
1.5 (S3)	11.11	8.36	11.58	–	0.11 (0.69)
2.0 (S4)	11.18	8.54	11.40	–	0.14 (0.92)

[a] The theoretical values are presented within parentheses.

core–shell structure (verified by TEM) with proper chemical bonds (verified by FTIR spectroscopy) favored more migration of fluorinated segments than the random copolymer structure thanks to the lower constraint to segmental motion in the shell layer for a lack of covalent and hydrogen-bonding force directly with the core.[22–24] Interestingly, no silicon was detected on the film–air surface of the core–shell latex film. It seemed that competition between fluorine and silicon atoms occurred during the surface self-segregation.[25]

To better understand the migration competition mechanism between the fluorine and silicon atoms, cross sections of the latex films were analyzed with SEM–EDX, and the results are listed in Table III. With various modified SiO_2 contents, the F amounts in the film bulk were always much lower than those in the film–air interface and film–glass interface, which decreased the surface energy, whereas silicon was always rich in the film–glass interface instead of the film–air interface; this was the result of many synthetic factors. Polarity was the main driving force among all of them because some hydroxyl groups remained on the modified SiO_2 surface [seen Fig. 4(c) of the FTIR analysis] and drove the modified SiO_2 onto the glass substrate with a similar polarity. In addition, the higher density of modified SiO_2 compared to that of the polymer matrix may have also driven the silicon particles to the glass substrate at bottom because of the action of gravity. However, a lower silicon content was even observed on the film–glass interface than the calculated theoretical value; this may have been to the shielding effect of the polymer coating on the surface of silicon particles.

Meanwhile, the variations of F amount on the film–air interface, which varied with different modified SiO_2 contents, were studied by the comparison of samples S1, S2, and S3, as shown in Table III. The F amounts on the film–air interface changed obviously from 10.55 to 11.11 wt % when the modified SiO_2 content ranged from 0.5 to 1.5 wt %. The F amount changed little from just 11.11 to 11.18 wt % with the increase in the modified SiO_2 content from 1.5 to 2.0 wt %. This confirmed that the fluorine migration toward the film–air interface was somewhat affected by the quantity addition of modified SiO_2, so there was a migration competition between F and Si. In the initial stage, the fluorine content increased comparatively on the film–air interface with the increase in the modified SiO_2 content. This was because the addition of more modified SiO_2 resulted in a large number of core–shell structure latex particles, which effectively enhanced the microphase separation and fluorine migration onto the film–air interface and, finally, made more fluorine rich in the film–air interface. However, such an increase in the fluorine content was not significant on the film–glass interface (just ranging from 11.4 to 11.58 wt %) with increasing modified SiO_2 content from 0.5 to 1.5 wt %, because silicon on the film–glass interface prevented the migration of fluorine onto the same position when the total translocation of fluorine and silicon reached a maximum value. However, the migrations of fluorine on the film–air and film–glass interface were both reduced with increasing modified SiO_2 content to 2.0 wt %. The superabundant modified SiO_2 had to migrate upward and, finally, affected the fluorine migration to the film–air interface when the fluorine content reached an optimum value on the film–glass interface. However, the silica core had little effect on the fluorine migration, especially to the film–air interface. We deduced from the SEM–EDX analysis that the self-assembly of the modified SiO_2 core, and the fluorinated segment chains occurred during film formation and produced a lower surface energy.

In conclusion, there was a real competition between fluorine and silicon during the surface self-segregation, and the distributions of F and Si content along the cross sections of the latex films exhibited a gradient to the surface; that is, fluorine-containing chains were localized on the film–air interface, and most silica particles lay on the film–glass interface during film formation. As expected, the orientation of F and Si played an important role in the properties of the films; these were suitable for the combination of latex with a protective substrate and gave a fluoroacrylate surface specialty, especially with a low surface energy.

To evaluate the excellent surface properties, which were expected, the static contact angle and surface

TABLE IV
Influence of the Contents of TFEMA on the Properties of the Film Surface

	Sample				
	N1	N2	N4	N5	N6
TFEMA content (wt %)	10	20	30	40	50
Water contact angle (°)	91	80	114	93	100
Hexadecane contact angle (°)	47	43	55	39	40
Surface energy (mN/m)	24.01	29.73	17.19	24.95	22.91

energy were determined by variation of the TFEMA and modified SiO_2 contents, as shown in Tables IV and V, respectively. As shown in Table IV, when the TFEMA content was increased under the same weight ratio of BA/MMA = 4/3 (ca. 1.333), the surface energy dramatically decreased first and then slightly increased. The surface free energy decreased to 17.19 mN/m when the TFEMA content was 30 wt %. Therefore, the film formed with a 30 wt % TFEMA content exhibited the most excellent hydrophobic properties. For TFEMA contents higher than 30 wt %, the contact angles and surface energies did not increase accordingly but decreased relatively; this resulted from the limitation of the migration of the fluorine atoms onto the film surface. As the migration reached a certain degree, the continuing migration was hindered by the steric effect of the fluorine atoms migrating to the film–air interface. In particular, compared to the film with 40 wt % TFEMA, there were slight increases in the contact angles and a slight decrease in the surface energy of the film with 50 wt % TFEMA. This contributed to the high TFEMA proportion in the shell polymer, which offset the adverse impact of the decrease in the shell polymer amount due to the increase in low-activity TFEMA on the enhancement of the surface properties of the film. In addition, the biggest surface free energy (29.73 mN/m) was measured for sample N2 because the BA/MMA weight ratio was a little lower (1.319).

As for the effect of the modified SiO_2 content on the properties of film, it revealed a nonlinear relation (Table V). A minimum surface energy (21.09 mN/m) was obtained with 1.0 wt % modified SiO_2. When the amount of modified SiO_2 was varied from 0.5 to 1.0 wt %, there was a reduction in the number of free polymer latex particles during the seed emulsion polymerization and an increase in the number of core–shell latex particles, so the proportion of fluorine in the shell polymer increased and resulted in a decrease in the surface energy from 21.75 to 21.09 mN/m. However, such an effect was limited with the increase of modified SiO_2 because the surplus modified SiO_2 likely caused coagulation of the latex particles, which caused a great activity loss for all of the monomers, especially low-activity TFEMA. This was bound to reduce the fluorine content of the final film material and the final surface energy. The changes in surface energy in samples S4 and S5 were not obvious (26.17 and 26.01 mN/m), and the results were consistent with the data obtained from SEM–EDX analysis. However, compared with the lesser influence of the modified SiO_2 content on the surface free energy (from 21.09 to 26.17 mN/m, as shown in Table V), the TFEMA content greatly affected the surface free energy, which ranged from 17.19 to 29.73 mN/m, as shown in Table IV, which further confirmed the orientation of F and Si during film formation. Actually, it was mainly the migration of fluorine-containing chains onto the film surface that made the films have higher static contact angles and a lower surface free energy. The film with optimal contents of TFEMA (30 wt %) and modified SiO_2 (1.0 wt %) indeed had extraordinary surface properties.

TABLE V
Influence of the Contents of Modified SiO_2 on the Properties of the Film Surface

	Sample				
	S1	S2	S3	S4	S5
Modified SiO_2 content (wt %)	0.5	1.0	1.5	2.0	2.5
Water contact angle (°)	100	102	97	90	91
Hexadecane contact angle (°)	45	46	43	38	37
Surface energy (mN/m)	21.75	21.09	22.94	26.17	26.01

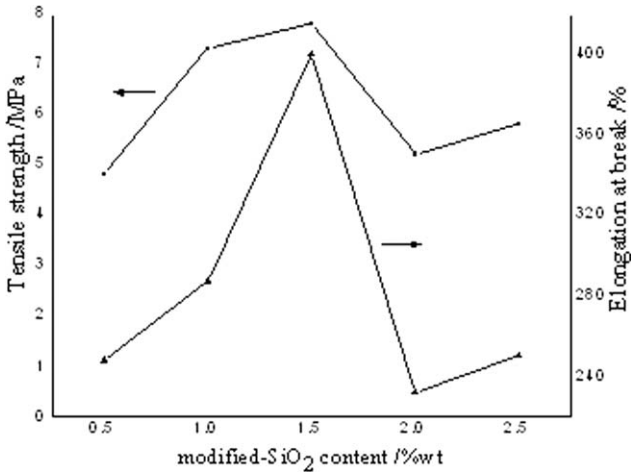

Figure 8 Effects of the content of modified SiO_2 on the tensile strength and elongation at break of the films.

Mechanical properties of the film

It is known that acrylic copolymers have less strength, so nano-SiO_2 become a major factor in the mechanical properties of latex films. For the purposes of investigating the function of modified SiO_2, the tensile strength and elongation at break values of films with different modified SiO_2 contents were investigated in this article (as shown in Fig. 8). In general, with increasing modified SiO_2 content, the tensile strength and elongation at break of the latex

films increased first and then decreased, except for those in sample S5. The modified SiO_2 reinforcing and toughening polymer matrix was mainly ascribed to nanoparticles in the bulk absorbing some of energy through crazes, whereas the film material bore an external mechanical force.

Specifically, the film with 1.0 wt % modified SiO_2 exhibited a higher tensile strength (7.3 MPa) than that with 0.5 wt % modified SiO_2 (4.8 MPa) because of the decrease in the number of neat polymer particles with increasing modified SiO_2 content; this agreed with the TEM images. However, the tensile strength with 1.5 wt % modified SiO_2 (7.8 MPa) was almost similar to that with 1.5 wt % modified SiO_2 (7.3 MPa). This suggested that the effect of modified SiO_2 on reinforcement and toughening was limited. When the modified SiO_2 content increased over 1.5 wt %, the tensile strength was not enhanced anymore. Because the aggregates of surplus modified SiO_2 in calabash shape [as shown in the TEM images in Fig. 2(c,d)] affected the heterogeneity of the whole film material, they finally caused a decline in the value of the tensile strength. When this content continued to grow from 2.0 to 2.5 wt %, the tensile strength increased slightly. This could have been related to a mass of rigid particles partly withstanding matrix cracking caused by irregular stress distribution. Similar to the variation of tensile strength, the maximum elongation at break (400%) was obtained for the latex film with 1.5 wt % modified SiO_2. From this point of view, the amount of modified SiO_2 should be controlled at 1.0–1.5 wt % to provide better mechanical properties.

CONCLUSIONS

Core–shell nano-SiO_2/P(MMA–BA–TFEMA) latexes were successfully obtained by seed emulsion polymerization with the help of a mixed emulsifier of TX-10 and SDS. The size distribution of the latex was homogeneous, and the average diameter of the core–shell latex particles was 45 nm. In the nano-SiO_2/P(MMA–BA–TFEMA) core–shell latex, the nano-SiO_2 and P(MMA–BA–TFEMA) were bridged by a VTMS coupling agent. The strong chemical bond improved the thermal properties of the films compared with the blending one.

The film obtained by the core–shell nano-SiO_2/fluorinated acrylic copolymer latex was actually a cocontinuous film, and the main elements on the film–air interface were carbon, oxygen, and fluorine. The fluorine content on the film surface was proportional to the TFEMA content and a little higher than the theoretical value, whereas silicon was detected on the film–glass interface. This was because the fluorine-containing chains migrated onto the film–air interface because of a decrease in surface energy, and the most silica particles tended to distribute in the region close to the film–glass interface in the combined effects of polarity and gravity during film formation. The self-assembly of the modified SiO_2 core and the fluorinated segments made the tightly packed $-CF_3$ groups on the film surface and rendered the fluorinated polymers particular low on surface free energy. Such an orientation of F and Si played an important role in the properties, such as the contact angles, surface energy, and mechanical properties, of the films.

When the TFEMA content was 30 wt %, favorable characteristics both in the latex and film properties were obtained because the content of fluorine on the film–air interface (18.48 wt %) was much higher than the theoretical value (10.18 wt %) because of the migration of fluorine to the film–air interface during film formation. The latex film with 1.0–1.5 wt % of modified nano-SiO_2 had better mechanical properties.

References

1. Rao, C. N. R.; Cheethan, A. K.; Thirumurugan, A. J Phys: Condens Matter 2008, 20, 83.
2. Haas, K. H. Adv Eng Mater 2000, 12, 571.
3. Zulfikar, M. A.; Mohammad, A. W.; Kadhum, A. A.; Hilal, N. Mater Sci Eng A 2007, 452, 422.
4. Ma, J. Z.; Hu, J.; Zhang, Z. J. Eur Polym J 2007, 43, 4169.
5. Cui, X. J.; Zhong, S. L.; Wang, H. Y. Polymer 2007, 48, 7241.
6. Freris, I.; Cristofori, D.; Riello, P.; Benedetti, A. J Colloid Interface Sci 2009, 331, 351.
7. Yu, Z. G.; Zhang, Z. B.; Yuan, Q. L.; Ying, S. K. Adv Polym Technol 2002, 21, 268.
8. Wang, H. X.; Fang, J.; Cheng, T.; Ding, J.; Qu, L. T.; Dai, L. M.; Wang, X. W.; Lin, T. Chem Commun 2008, 7, 877.
9. Sasazawa, K.; Kurachi, J.; Narumi, T.; Nishi, H.; Yamamoto, Y.; Sawada, H. J Appl Polym Sci 2007, 103, 110.
10. Li, Y.; Yang, T. T.; Cheng, S. Y. Acta Polym Sinica 2008, 3, 221.
11. He, L.; Liang, J. Y. J Fluorine Chem 2008, 129, 590.
12. Qu, A. L.; Wen, X. F.; Pi, P. H.; Cheng, J.; Yang, Z. R. J Colloid Interface Sci 2008, 317, 62.
13. Shi, X. M.; Xu, S. M.; Lin, J. T.; Feng, S.; Wang, J. D. Mater Lett 2009, 63, 527.
14. Li, X. H.; Cao, Z.; Zhang, Z. J.; Dang, H. X. Appl Surf Sci 2006, 252, 7856.
15. Wen, X. F.; Li, M. Z.; Pi, P. H.; Chen, J.; Yang, Z. R. Colloids Surf A 2008, 327, 103.
16. Collinson, M. M. Mikrochim Acta 1998, 129, 149.
17. Kim, J. M.; Chang, S. M.; Kim, S.; Kim, K.; Kim, J.; Kim, W. Ceram Int 2009, 35, 1243.
18. Qu, A. L.; Wen, X. F.; Pi, P. H.; Cheng, J.; Yang, Z. R. Colloids Surf A 2009, 345, 18.
19. Zou, H.; Wu, S. S.; Shen, J. Chem Rev 2008, 108, 3893.
20. Kashiwagi, T.; Morgan, A. B.; Antonucci, J. M.; VanLandingham, M. R.; Harris, R. H.; Awad, W. H.; Shields, J. R. J Appl Polym Sci 2003, 89, 2072.
21. Cui, X. J.; Zhong, S. L.; Zhang, H.; Wang, H. Y. Colloids Surf A 2007, 303, 173.
22. Cheng, S. Y.; Chen, Y. J.; Chen, Z. G. J Appl Polym Sci 2002, 85, 1147.
23. Fabbri, P.; Messori, M.; Montecchi, M.; Nannarone, S.; Pasquali, L.; Pilati, F.; Tonelli, C.; Toselli, M. Polymer 2006, 47, 1055.
24. Xiao, X. Y.; Liu, J. F. Chin J Chem Eng 2008, 16, 626.
25. Tsibouklis, J.; Nevell, T. G. Adv Mater 2008, 15, 7.